[논 문] 한국재료학회지
Korean Journal of Materials Research
Vol. 5, No. 2 (1995)

The Determination of Stress Distribution in WC-Ni Cemented Carbide Composites by Neutron Diffraction

Kyeongwon Seol

Dept. of Metallurgical Eng., Chonbuk National University, chonju, 560-756

Abstract The thermal stress distribution of WC and Ni binder phases in WC-26wt.%Ni and WC-6wt.%Ni composites has been investigated over the temperature range 100-900 K using a time-of-flight neutron diffractometer. To determine the stress distribution, the breadths of WC and Ni peaks in the reference powder and the composites were analyzed. The peak breadths were corrected for particle size effect using a procedure based on the integral peak breadth method of particle size-strain analysis. The result shows a broad range of strain, and thus stress, is present in the WC and Ni binder phases of the composites. The strain distribution of both phases broadens as the temperature decreases, and some fraction of total strain distribution of the WC phase remains tensile regardless of the temperature. The strain distribution of the WC phase broadens as the binder content increases, and that of Ni binder phase broadens as the binder content decreases, which means the strain distribution broadens as the absolute value of residual stress increases.

1. INTROUDUCTION

Numerous studies on the differential thermal stress state in cemented carbide composites have been performed using X-rays[1-5] and neutrons[6-8]. Although the quantitative validity of the x-ray studies has been questioned, they have generally shown the presence of compressive carbide and tensile binder stress. Furthermore, some of the recent works have documented changes in the stress state due to cyclic and monotonic compression, with attendant changes in Palmqvist crack length[5,6].

However, almost none of the experimental works to date have dealt with the variance or distribution of the residual stresses around their average values. In addition to stress gradient in the vicinity of binder-carbide interfaces as a consequence of the need to maintain continuity across boundaries, other contributors to the variance are possible. Those are carbide morphology, carbide particle size, and carbide content. The broadening of the powder pattern peaks of the material is normally caused by small crystallite size and by distortions within the crystallites. In addition, the experimental diffraction geometry contributes to peak broadening. If the observed line profiles corrected for instrumental broadening are expressed as Fourier series, then an analysis of the Fourier coefficients enables determination of both particle size and strain contributions, without the necessity of any prior assumptions. The first measurements of this kind were made by Warren and Averbach[9] and similar studies followed. Recently has the variance or distribution of stresses been investigated[7,10]. Those results indicated that the stress distrubution is broader for angular relative to the round carbide and for lower relative to higher carbide contents. Thus, it appears that the breadth of stress distrubution increases with carbide angularity and with the binder content.

In the present study, strain distributions in both WC and Ni binder phases has been obtained from model WC-Ni cemented carbide particulate composites as a function of temperature. Measurements were done by the high resolution powder diffractometer[11] at the Ar-

gonne Intense Pulsed Neutron Source, and the breadths of WC and Ni peaks in the composites were analyzed using a procedure based on the integral peak breadth method of particle size-strain analysis.

2. EXPERIMENTAL DETAILS

2.1 Specimens

WC-26wt.%Ni and WC-6wt.%Ni cemented carbide composites were used for this study. They were made by liquid phase sintering at 1440℃ for low binder composite and at 1350 ℃ for high binder composite. Instead of commercial WC-Co, model WC-Ni composites were used in this study because Ni is more stable than Co as a binder and more visible due to a large neutron scattering crosssection compared to Co. Composites are rectangualr parallelpipeds with approximate dimensions of $0.65 \times 0.65 \times 6.4$cm. Krawitz[12] found that the FWHM(Full Width at Half Maximum) values of annealed WC powder are essentially same as those of annealed Si powder used to obtain instrumental peak shape parameters. Thus, annealed WC powder was used for the correction of the instrumental broadening for integral peak breadth analysis as well as for the strain -free reference standards. Annealed Ni powder was also used to determine the strain distribution in the binder phase.

2.2 Equipments and Measurements

All the measurements for the stress distribution of WC-Ni composites were carried out using the General Purpose Powder Diffractometer (GPPD) at the Argonne Intense Pulsed Neutron Source (IPNS). The GPPD is a high resolution time-of-flight (TOF) neutron scattering instrument. Banks of detectors are arranged at a constant scattered flight path distance (1.5m) from the sample position, and are located symmetrically on either side of the incident beam at nominal scattering angles of $2\theta = 151.8$, 90, 60, and 30°.

With the detectors fixed, the GPPD uses the time-of-flight of the neutrons to determine the various wavelength components. Since determination of stress distribution requires the precise measurement of the breadths of several peaks, the time-of-flight technique is particularly advantageous for this experiments. The spectrum is measured at a fixed Bragg angle of $2\theta = 148°$. A cryo-refrigerator was used for low temperature measurements and a Ta-resistance furnace for high temperature measurements over the temperature range 100-900K. A vacuum of an order of 10^{-6}torr was used for low and high temperature measurements, and about 10^{-5}torr was used for room temperature measurements.

Composites were put into vanadium cans and attached to the top of the can using epoxy resin to fix the sample position. Cans were sealed in He atmosphere to improve the thermal conductivity for low temperature measurements. For high temperature measurements He atmosphere was not used because it makes the vacuum condition worse. Samples were carefully positioned such that one face of the rectangular cross section was perpendicular to the incident beam to reduce absorption problem which can occur due to shift or rotation of the samples. Identical measurements were made on the WC and Ni standard powders. Powders were put into the same vanadium can to reduce the absorption problem between the composites and powders.

3. RESULTS AND DISCUSSION

3.1 Peak Breadth

FWHM values of the WC and Ni binder phases were obtained using the TOFMANY[13] computer program for single peak profile analysis at IPNS. The GPPD peaks are asymmetric in shape and can be characterized by a convolution of exponential leading and lagging tails with a Gaussian. There are seven parameters which define the shape and position of any peak : two for the magnitude of

the background on either side of the peak, two for the exponential tails, one for the mean peak position, one for the FWHM of the Gaussian, and one for the scale or height of the peak. For this analysis, seven WC peaks and five Ni binder peaks were used. Those were 100, 101, 110, 002, 201, 112, 300 for the WC and 111, 200, 311, 222, 331 for the Ni binder phases. After examining the entire spectrum of the composite, these peaks were chosen as the most appropriate because they had enough intensity and were not overlapped with other peaks.

The plots of the Gaussian FWHM for the WC 201 and Ni 311 peaks in the WC-26wt.% Ni and WC-6wt.%Ni composites are shown as a function of temperature in Fig. 1. The WC

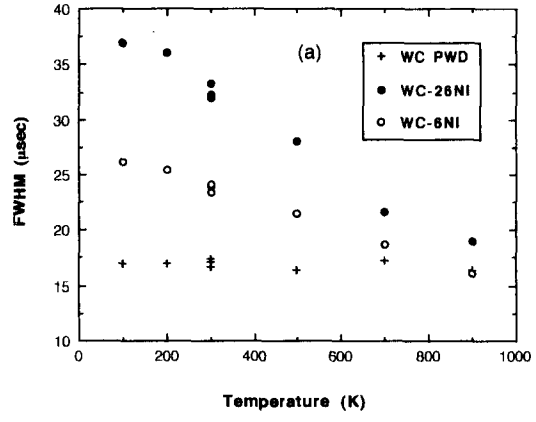

Fig. 1. The FWHM values of the (a) WC phase and (b) Ni binder phase in the composites and the standard powder.

powder gives the peak breadths that are essentially the same as those of the annealed silicon powder standard[10], so the WC powder is used to correct the instrumental peak broadening. On the other hand, the FWHM values of the WC and Ni phases in the composites are markedly broadened at low temperature and sharpen as temperature increases, i.e. as the residual stress decreases. The FWHM values of the WC phase are smaller in the WC-6wt.% Ni than in the WC-26wt.%Ni composite. However, those of the Ni binder phase are smaller in the WC-6wt.% Nl composite. Thus, the peak breadths are greatly affected by the residual stresses in the composites, i.e. the FWHM values increased as the residual stress increased.

3.2 Strain Distribution

The strain distribution is calculated by the modified integral peak breadth analysis[9,10]. Instead of integral peak breadths, Gaussian FWHM values which are returned by the peak fitting programs are used. The basic aspects of this method are summarized below. The peak breadth, now termed B, is the FWHM value of the composite after correction for instrumental breadth, i.e.

$$B^2 = B^2_{meas} - B^2_{stan} \quad (1)$$

where B_{meas} is the FWHM value measured for the composite and B_{stan} is the value for the standard. This correction procedure assumes that all peak shapes are Gaussian. The breadth B consists of a particle size component B_D and a strain component B_S. For the case where all sources of broadening are also Gaussian, the appropriate equation is[7]

$$B^2 = B^2_D + B^2_S = (\lambda/D\cos\theta)^2 + (4<\varepsilon>\tan\theta)^2 \quad (2)$$

where λ is neutron wavelength, D is the particle size, θ is the diffraction angle, and $<\varepsilon>$ is the variance of the strain in the material. The terms on the right hand side of eq. (2) correspond to particle size and strain, respectively.

Rearranging eq. (2) gives the following relationship.

$$(B\cos\theta/\lambda)^2=(1/D)^2+(4<\varepsilon>\sin\theta/\lambda)^2 \quad (3)$$

However, the FWHM values obtained from the GPPD are given in time-of-flight units, so this equation should be converted into time-of-flight units instead of λ using the equation, $\lambda = ht/mL = 2d\sin\theta$. Thus, the basic equation for the peak breadth analysis can be expressed as eq.(4)[9].

$$\left(\frac{\triangle t}{t}\right)^2=\left(\frac{h}{2DmL\sin\theta}\right)^2t^2+(4<\varepsilon>)^2 \quad (4)$$

where h is Planck's constant, t is the time taken for a neutron to travel the total flight path L, d is the interplanar spacing, and m is the mass of the neutron. In this equation, the breadth ($\triangle t$) is the FWHM value of the composite after correction for instrumental breadth, i.e.

$$\triangle t^2=\triangle t^2_{meas}-\triangle t^2_{stan} \quad (5)$$

Where $\triangle t_{meas}$ is the FWHM value measured for the composite and $\triangle t_{stan}$ is the value for the standard calculated from that of the WC powder. The FWHM value of the WC powder varies with the peak positions, so all the FWHM values are plotted as a function of the time-of-flight (t), and the linear least square fit is performed. The results are given in Fig. 2. The experimental values are fit well with the equation and it is used to obtain the standard FWHM values for each peak.

Plots of $\left(\frac{\triangle t}{t}\right)^2$ vs. t^2 for the WC and Ni binder phases show similar trends. The typical plots for the WC-26wt.%Ni at 300K are shown in Fig. 3. Although some of the FWHM values in the composite are smaller than those of the standard at 900K, they were assumed to have the same values as those of the standard. Strain variance and particle size were calculated from the intercept and the slope of the line fitted using methods of least squares, respectively. The calculated particle size (mosaic size) has an order of several thousand angstroms. This means that the mosaic size

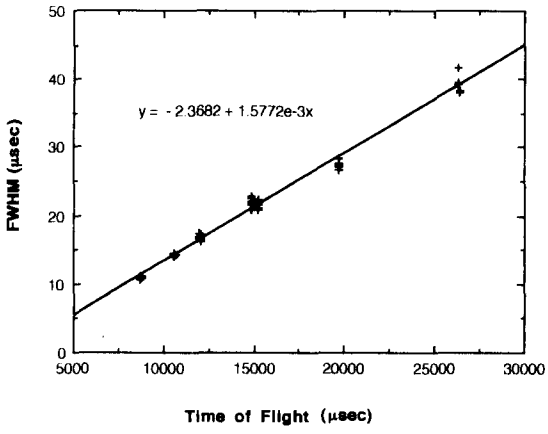

Fig. 2. The change of FWHM values of the WC powder with the peak position.

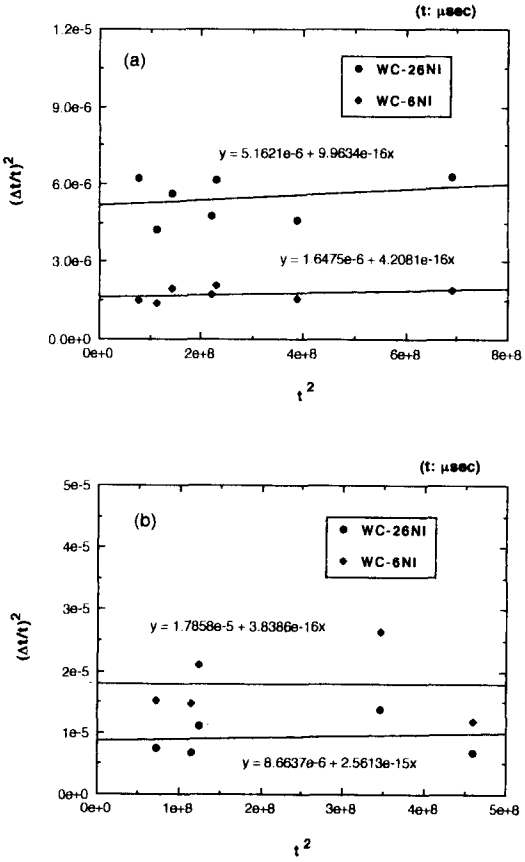

Fig. 3. Typical plots of $\left(\frac{\triangle t}{t}\right)^2$ vs. t^2 for the (a) WC phase and (b) Ni binder phase of the WC-26wt.%Ni composite at 300K.

measured by diffraction is a substantial fraction of the actual particle size(a few microns).

Drake[4] reported that the dislocation densities in the WC and Ni phases for as-produced WC-Ni composites are 10^7-10^8 and 10^8-10^9cm $^{-2}$, respectively. These values of the dislocation densities are similar as those of fully annealed metals, so it can be safely assumed that the microstrain effects as a consequence of the dislocations do not affect the peak broadening for the composites used for the present study. Thus, it can be concluded that the measured strain distribution does not result from microstrain as in cold-worked metals or alloys, but from a distribution of elastic strain arising from a local variation in the elastic residual stress.

The value of the strain variance obtained from this analysis can be used to generate a strain distribution, assuming a Gaussian behavior, by the following equation[10] :

$$f(\varepsilon)=\frac{1}{s(2\pi)^{1/2}}\exp\left\{-\frac{1}{2}\left(\frac{\varepsilon-\varepsilon_0}{s}\right)^2\right\} \quad (6)$$

where $f(\varepsilon)$ is a strain distribution normalized based on the unit area, ε_0 is the mean strain value[14], and s is standard deviation, which is related to the strain variance by

$$<\varepsilon>=2(2\ln 2)^{1/2}\cdot s \quad (7)$$

The resultant Gaussian strain distributions of the WC and Ni phases for the WC-26wt.%Ni composite are presented in Fig. 4 as a function of temperature.

Both the WC and Ni binder phases show similar trends, i.e. the strain distribution broadens as the temperature decreases. In the case of the WC phase, some fraction of the total strain distribution remains tensile regardless of the temperature. However, this does not necessarily mean that there is tensile stress in the sample, because the strain distribution can not be converted into the stress distribution directly. There seem to be two sources for the strain (stress) distribution : the angularity of the WC particles and the distribution of the WC particles with various aspect ratios. Separation of these two effects, however, appears to be difficult.

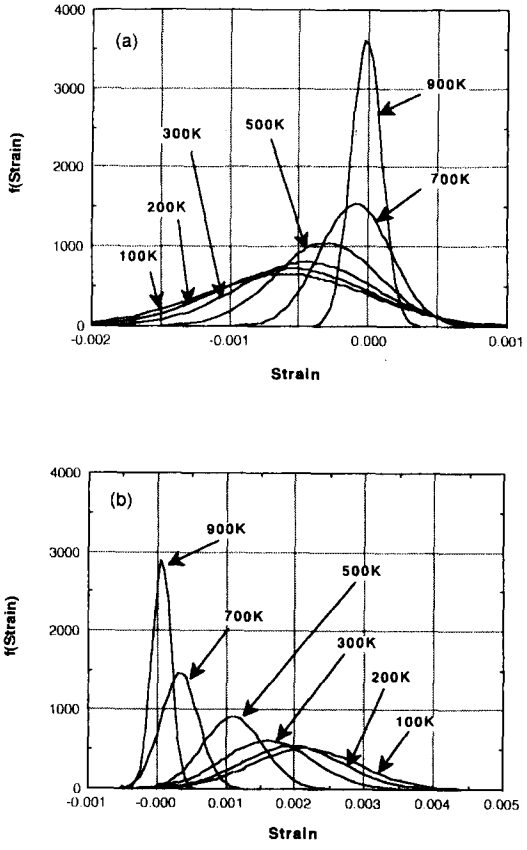

Fig. 4. The strain distributions of the (a) WC phase and (b) Ni phase for the WC-26wt.%Ni composite as a function of temperature.

The experimentally determined strain distributions of the WC and Ni phases in the composites at 300K are presented in Fig. 5. The strain distribution broadens as the binder content increases for the WC phase. This is to be expected, because the high binder composite contains more compressive stress than the low binder one[14]. The percentages of the tensile strains are 16.3 and 17.3% for WC-26wt.%Ni and WC-6wt.%Ni, respectively. Even though this does not directly mean there is the same fraction of tensile stresses, the low binder composite shows a greater possibility of a large

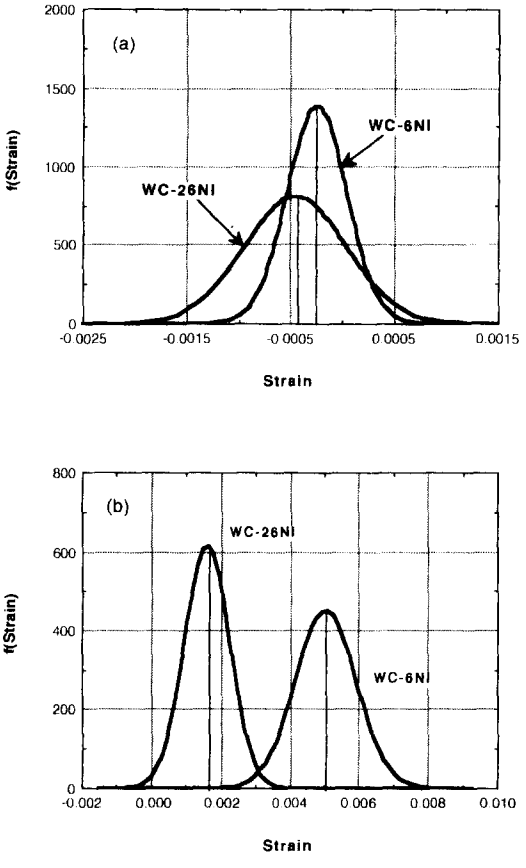

Fig. 5. The experimentally determined strain distributions of the (a) WC phase and (b) Ni phase in the composites at 300K.

fraction of tensile stress than the high binder one.

In the case of Ni binder phase, the low binder composite shows a broader strain distribution than the high binder one. This is consistent with the results of the WC phase. As the tensile stress of the binder phase increases, the strain distribution broadens. However, the Ni binder phase does not exhibit compressive strain.

3.3 Stress Distribution

Krawitz[7] directly converted the strain distribution into the stress distribution assuming that all strain distributions are due to the angularity of WC particles, i.e. they have a hydrostatic nature. However, the distribution of the WC particles with various aspect ratios is also a source for strain distribution. It has an anisotropic nature so that it cannot be converted into the stress distribution easily. An other trouble for the conversion of the strain distribution into the stress distribution is that the fraction of each effect to the total strain distribution of the real sample is not known.

Krawitz assumed only one source of strain distribution and also normalized the Gaussian function based on unit height instead of unit area. Thus, the absolute stress values given by them are questionable. Recently, Majumdar[10] calculated the stress distribution of the WC phase in a WC-Ni composite by the finite element method (FEM) with triangular and rectangular particle shapes. Although the calculation is two-dimensional, the calculated stress distribution is much narrower than that obtained by Krawitz. Thus, absolute values of stress distribution obtained by Krawitz assuming one source of strain distribution should be corrected.

Fig. 6 shows the typical Gaussian plots for stress distribution of the WC phase in the composites at 300K. These plots are obtained assuming that the stress distribution is due solely to the angularity of the WC particles, which is same assumption used by Krawitz. As shown in Fig. 6, the stress distribution is broader as the absolute magnitude of stress increases. Although it is difficult to say quantitatively, the actual composites possibly have some fraction of tensile stress. A more accurate three-dimensionl FEM model and quantitative metallography may be needed for a better quantitative analysis.

4. CONCLUSTIONS

The strain distributions of WC and Ni binder phases in WC-26wt.%Ni and WC-6wt.%Ni composites have been determined experimentally. The result shows a broad range of strain, and thus stress, is present in the WC and Ni binder phases of the compos-

ites. The strain distribution broadens as the temperature decreases and some fraction of the total strain distribution of the WC phase remains tensile regardless of the temperature. The strain distribution of the WC phase broadens as the binder content increases and that of Ni binder phase broadens as the binder content decreases. This means the strain distribution broadens as the absolute value of stress increases. Although it is difficult to say quantitatively, the actual composites show a possibility to have some fraction of tensile stress.

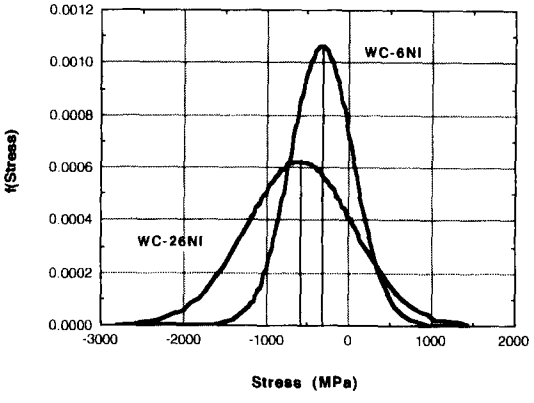

Fig. 6. Typical Gaussian plots for stress distribution of the WC phase in the composites at 300K.

REFERENCES

1. J. Gurland, Trans. am. Soc. Met., 50 (1958) 1063-1071.
2. D.N. French, J. Am. Ceram. Soc., 52 (1969) 267-271, 271-275.
3. B.O. Jaensson, Mater. Sci. Eng., 8 (1971) 41-53.
4. E.F. Drake and A.D. Krawitz, Met. Trans., 12A (1981) 505-513.
5. G. Vekinis and B. Luyckx, 2nd Int. Conf. on the Science of Hard Materials, 75 (1984) 591-600.
6. A.D. Krawitz, R. Roberts, and J. Faber, 2nd Int. Conf. on the Science of Hard Material, 75 (1984) 577-589.
7. A.D. Krawitz, M.L. Krapenhoft, D.G. Reichel, and R. Warren, Mater. Sci. Eng., A105-106 (1988) 275-281.
8. K. Seol and A.D. Krawitz, Mater. Sci. Eng., A127 (1990) 1-5.
9. B.L. Averbach and B.E. Warren, J. Appl. Phys., 20 (1949) 885-886.
10. A.D. Krawitz, D.G. Reichel, and R.L. Hitterman, Mater. Sci. Eng., A119 (1989) 127-134.
11. J.M. Carpenter and G.H. Lander, Review of Scientific Instruments, 55 (1984) 1019-1043.
12. A.D. Krawitz, D.G. Reichel, and R.L. Hitterman, J. Am. Ceram. Soc., 72 (1989), 515-517
13. S.R. MacEwen, J. Faber, and A.P.L. Turner, Acta Metall., 31 (1983) 657-676.
14. K. Seol(submitted to J. Korean Inst. Met. Mater.).
15. S. Majumdar, D. Kuppermann, and J. Singh, J. Am. Ceram. Soc., 71 (1988) 858-863.